# Precise measurement of spin-averaged $\chi_{cJ}(1P)$ mass using photon conversions in $\psi(2S) \to \gamma\chi_{cJ}$

M. Ablikim,[1] J. Z. Bai,[1] Y. Ban,[11] J. G. Bian,[1] X. Cai,[1] J. F. Chang,[1] H. F. Chen,[17] H. S. Chen,[1] H. X. Chen,[1] J. C. Chen,[1] Jin Chen,[1] Jun Chen,[7] M. L. Chen,[1] Y. B. Chen,[1] S. P. Chi,[2] Y. P. Chu,[1] X. Z. Cui,[1] H. L. Dai,[1] Y. S. Dai,[19] Z. Y. Deng,[1] L. Y. Dong,[1,*] Q. F. Dong,[15] S. X. Du,[1] Z. Z. Du,[1] J. Fang,[1] S. S. Fang,[2] C. D. Fu,[1] H. Y. Fu,[1] C. S. Gao,[1] Y. N. Gao,[15] M. Y. Gong,[1] W. X. Gong,[1] S. D. Gu,[1] Y. N. Guo,[1] Y. Q. Guo,[1] Z. J. Guo,[16] F. A. Harris,[16] K. L. He,[1] M. He,[12] X. He,[1] Y. K. Heng,[1] H. M. Hu,[1] T. Hu,[1] G. S. Huang,[1,†] X. P. Huang,[1] X. T. Huang,[12] X. B. Ji,[1] C. H. Jiang,[1] X. S. Jiang,[1] D. P. Jin,[1] S. Jin,[1] Y. Jin,[1] Yi Jin,[1] Y. F. Lai,[1] F. Li,[1] G. Li,[2] H. H. Li,[1] J. Li,[1] J. C. Li,[1] Q. J. Li,[1] R. Y. Li,[1] S. M. Li,[1] W. D. Li,[1] W. G. Li,[1] X. L. Li,[8] X. Q. Li,[10] Y. L. Li,[4] Y. F. Liang,[14] H. B. Liao,[6] C. X. Liu,[1] F. Liu,[6] Fang Liu,[17] H. H. Liu,[1] H. M. Liu,[1] J. Liu,[11] J. B. Liu,[1] J. P. Liu,[18] R. G. Liu,[1] Z. A. Liu,[1] Z. X. Liu,[1] F. Lu,[1] G. R. Lu,[5] H. J. Lu,[17] J. G. Lu,[1] C. L. Luo,[9] L. X. Luo,[4] X. L. Luo,[1] F. C. Ma,[8] H. L. Ma,[1] J. M. Ma,[1] L. L. Ma,[1] Q. M. Ma,[1] X. B. Ma,[5] X. Y. Ma,[1] Z. P. Mao,[1] X. H. Mo,[1] J. Nie,[1] Z. D. Nie,[1] S. L. Olsen,[16] H. P. Peng,[17] N. D. Qi,[1] C. D. Qian,[13] H. Qin,[9] J. F. Qiu,[1] Z. Y. Ren,[1] G. Rong,[1] L. Y. Shan,[1] L. Shang,[1] D. L. Shen,[1] X. Y. Shen,[1] H. Y. Sheng,[1] F. Shi,[1] X. Shi,[11,‡] H. S. Sun,[1] J. F. Sun,[1] S. S. Sun,[1] Y. Z. Sun,[1] Z. J. Sun,[1] X. Tang,[1] N. Tao,[17] Y. R. Tian,[15] G. L. Tong,[1] G. S. Varner,[16] D. Y. Wang,[1] J. Z. Wang,[1] K. Wang,[17] L. Wang,[1] L. S. Wang,[1] M. Wang,[1] P. Wang,[1] P. L. Wang,[1] S. Z. Wang,[1] W. F. Wang,[1,§] Y. F. Wang,[1] Z. Wang,[1] Z. Y. Wang,[1] Zhe Wang,[1] Zheng Wang,[2] C. L. Wei,[1] D. H. Wei,[1] N. Wu,[1] Y. M. Wu,[1] X. M. Xia,[1] X. X. Xie,[1] B. Xin,[8,†] G. F. Xu,[1] H. Xu,[1] S. T. Xue,[1] M. L. Yan,[17] F. Yang,[10] H. X. Yang,[1] J. Yang,[17] Y. X. Yang,[3] M. Ye,[1] M. H. Ye,[2] Y. X. Ye,[17] L. H. Yi,[7] Z. Y. Yi,[1] C. S. Yu,[1] G. W. Yu,[1] C. Z. Yuan,[1] J. M. Yuan,[1] Y. Yuan,[1] S. L. Zang,[1] Y. Zeng,[7] Yu Zeng,[1] B. X. Zhang,[1] B. Y. Zhang,[1] C. C. Zhang,[1] D. H. Zhang,[1] H. Y. Zhang,[1] J. Zhang,[1] J. W. Zhang,[1] J. Y. Zhang,[1] Q. J. Zhang,[1] S. Q. Zhang,[1] X. M. Zhang,[1] X. Y. Zhang,[12] Y. Y. Zhang,[1] Yiyun Zhang,[14] Z. P. Zhang,[17] Z. Q. Zhang,[5] D. X. Zhao,[1] J. B. Zhao,[1] J. W. Zhao,[1] M. G. Zhao,[10] P. P. Zhao,[1] W. R. Zhao,[1] X. J. Zhao,[1] Y. B. Zhao,[1] Z. G. Zhao,[1,‖] H. Q. Zheng,[11] J. P. Zheng,[1] L. S. Zheng,[1] Z. P. Zheng,[1] X. C. Zhong,[1] B. Q. Zhou,[1] G. M. Zhou,[1] L. Zhou,[1] N. F. Zhou,[1] K. J. Zhu,[1] Q. M. Zhu,[1] Y. C. Zhu,[1] Y. S. Zhu,[1] Yingchun Zhu,[1,¶] Z. A. Zhu,[1] B. A. Zhuang,[1] X. A. Zhuang,[1] and B. S. Zou[1]

(BES Collaboration)

[1]*Institute of High Energy Physics, Beijing 100049, People's Republic of China*
[2]*China Center for Advanced Science and Technology (CCAST), Beijing 100080, People's Republic of China*
[3]*Guangxi Normal University, Guilin 541004, People's Republic of China*
[4]*Guangxi University, Nanning 530004, People's Republic of China*
[5]*Henan Normal University, Xinxiang 453002, People's Republic of China*
[6]*Huazhong Normal University, Wuhan 430079, People's Republic of China*
[7]*Hunan University, Changsha 410082, People's Republic of China*
[8]*Liaoning University, Shenyang 110036, People's Republic of China*
[9]*Nanjing Normal University, Nanjing 210097, People's Republic of China*
[10]*Nankai University, Tianjin 300071, People's Republic of China*
[11]*Peking University, Beijing 100871, People's Republic of China*
[12]*Shandong University, Jinan 250100, People's Republic of China*
[13]*Shanghai Jiaotong University, Shanghai 200030, People's Republic of China*
[14]*Sichuan University, Chengdu 610064, People's Republic of China*
[15]*Tsinghua University, Beijing 100084, People's Republic of China*
[16]*University of Hawaii, Honolulu, Hawaii 96822, USA*
[17]*University of Science and Technology of China, Hefei 230026, People's Republic of China*
[18]*Wuhan University, Wuhan 430072, People's Republic of China*
[19]*Zhejiang University, Hangzhou 310028, People's Republic of China*
(Received 6 February 2005; published 11 May 2005)

Using photon conversions to $e^+e^-$ pairs, the energy spectrum of inclusive photons from $\psi(2S)$ radiative decays is measured with photon energy resolution ($\sigma_{E_\gamma}$) in the range from 2.3 to 3.8 MeV by BESII at the

*Present address: Iowa State University, Ames, IA 50011-3160, USA.
†Present address: Purdue University, West Lafayette, IN 47907, USA.
‡Present address: Cornell University, Ithaca, NY 14853, USA.
§Present address: Laboratoire de l'Accélératear Linéaire, F-91898 Orsay, France.
¶Present address: DESY, D-22607, Hamburg, Germany.
‖Present address: University of Michigan, Ann Arbor, MI 48109, USA.

 

Beijing Electron-Positron Collider. The $\chi_{cJ}(1P)$ states ($J = 0, 1, 2$) are clearly observed, and their masses and the spin-averaged $\chi_{cJ}$ mass are determined to be $M_{\chi_{c0}} = 3414.21 \pm 0.39 \pm 0.27$, $M_{\chi_{c1}} = 3510.30 \pm 0.14 \pm 0.16$, $M_{\chi_{c2}} = 3555.70 \pm 0.59 \pm 0.39$, and $M(^3P_{\rm cog}) = 3524.85 \pm 0.32 \pm 0.30\ {\rm MeV}/c^2$, respectively.

DOI: 10.1103/PhysRevD.71.092002 PACS numbers: 14.40.Gx, 12.38.Qk, 13.25.Gv, 13.40.Hq

## I. INTRODUCTION

Precise measurements of the spectrum and the decay properties of charmonia are essential to test potential QCD models and QCD-based approaches [1]. There is renewed interest in this field since the discovery of the X(3872) [2] and the recent observations of the expected $\eta_c(2S)$ and $h_c(^1P_1)$ states [3], and there has been both theoretical and experimental progress in past years [4]. There are more accurate predictions of the charmonium mass spectrum and radiative transition rates using both a relativistic quark model with relativistic corrections of order $v^2/c^2$ [5] and a potential model with a semirelativistic approach [6]. The $\psi(2S)$ mass and width have been redetermined with an updated radiative correction [7] and newly measured with better precision [8]. In addition to previous measurements of $\chi_{cJ}$ states [9], two $\chi_{c0}$ measurements by E835 [10] and new $\chi_{cJ}$ ($J = 0, 1, 2$) measurements by CLEO [11] have been recently published. Improved precision on $\chi_{cJ}$ masses is important for the determination of the singlet-triplet splitting, $M(^1P_1) - M(^3P_{\rm cog})$, which is predicted by lattice QCD and nonrelativistic QCD [12]. Here $M(^3P_{\rm cog})$ is the spin-averaged $^3P_J$ mass for the $\chi_{cJ}$ states ($J = 0, 1, 2$).

In this paper, results on the $\chi_{cJ}$ masses ($J = 0, 1, 2$) and widths ($J = 0, 1$) from a measurement of the energy spectrum of inclusive photons in $\psi(2S)$ radiative decays, using photon conversions to improve the energy resolution, are presented. This measurement uses $14 \times 10^6$ $\psi(2S)$ events collected with the upgraded Beijing Spectrometer (BESII) at the Beijing Electron-Positron Collider (BEPC).

## II. BES DETECTOR AND MONTE CARLO SIMULATION

The BESII detector is described elsewhere [13]. A 12-layer vertex chamber (VC) surrounding the beam pipe provides hit and trigger information for charged tracks. Charged particle momenta are determined with a resolution of $\sigma_p/p = 1.78\%\sqrt{1 + p^2}$ ($p$ in GeV/$c$) in a 40-layer cylindrical drift chamber (MDC). Particle identification is accomplished by measurements of ionization ($dE/dx$) in the MDC and time-of-flight (TOF) in a barrel-like array of 48 scintillation counters. The $dE/dx$ resolution is $\sigma_{dE/dx} = 8\%$; the TOF resolution is $\sigma_{\rm TOF} = 200$ ps for hadrons. A 12-radiation-length barrel shower counter (BSC) measures energies of photons with a resolution of $\sigma_E/E = 21\%/\sqrt{E}$ ($E$ in GeV). A solenoidal coil supplies a 0.4 Tesla magnetic field over the tracking volume.

The event trigger for $\psi(2S)$ data requires at least one charged track and total energy deposit in the BSC $E_{\rm tot} \geq 100$ MeV for the multiprong event trigger and at least one neutral cluster with energy greater than 80 MeV and total energy deposit in the BSC $E_{\rm tot} \geq 800$ MeV for the neutral event trigger. For a charged track, at least one hit in both the VC and the TOF and one MDC track are required [14].

A GEANT3 based Monte Carlo (MC) BESII simulation program [15], which simulates the detector response including interactions of secondary particles in the detector material, is used to determine the energy resolution and detection efficiency of photons reconstructed from their converted $e^+e^-$ pairs, as well as to optimize selection criteria and estimate backgrounds. Under the assumption of a pure E1 transition for the $\psi(2S) \to \gamma\chi_{cJ}$ decays, the polar angle ($\theta$) distributions of the photons are given by $1 + k\cos^2\theta$ with $k = 1, -\frac{1}{3}, \frac{1}{13}$ for $J = 0, 1, 2$, respectively [16].

Good energy resolution for low energy photons is essential for precise $\chi_{cJ}$ mass and width measurements using the photon spectrum of $\psi(2S)$ radiative decays. Photons from $\psi(2S) \to \gamma\chi_{cJ}$ decays have energies of 261, 171, and 128 MeV for the $\chi_{cJ}$ final states ($J = 0, 1, 2$), and the electrons produced in their photon conversions have momenta from 60 to 250 MeV/$c$ and momentum resolution ($\sigma_p$) from 1.6 to 4.1 MeV/$c$.

## III. PHOTON RECONSTRUCTION AND SELECTION

We choose two oppositely charged tracks with each track having a good helix fit and a polar angle with $|\cos\theta| < 0.8$. The intersection of the two trajectories in the $xy$ plane (the beam line is the $z$ axis) is determined, and this point is taken as the photon conversion point (CP). The photon conversion length $R_{xy}$ is defined as the distance from the beam line to the CP in the $xy$ plane. Figure 1 shows the $R_{xy}$ distribution for candidate photon conversions to $e^+e^-$ pairs in the BESII detector for hadronic events in the $58 \times 10^6$ $J/\psi$ event sample. The two broad peaks in Fig. 1 correspond to the beam-pipe region, where the beam pipe, the VC, and inner wall of the MDC are located. Combinatorial background from charged hadron tracks is also seen in the $R_{xy} < 2$ cm region. Equivalent materials in the beam-pipe wall, VC, VC outer wall, and the MDC inner wall are 0.536, 0.657, 0.375, and 1.107 in units of $0.01X_0$ [17], respectively, where $X_0$ is a radiation length. The electron and positron directions are calculated

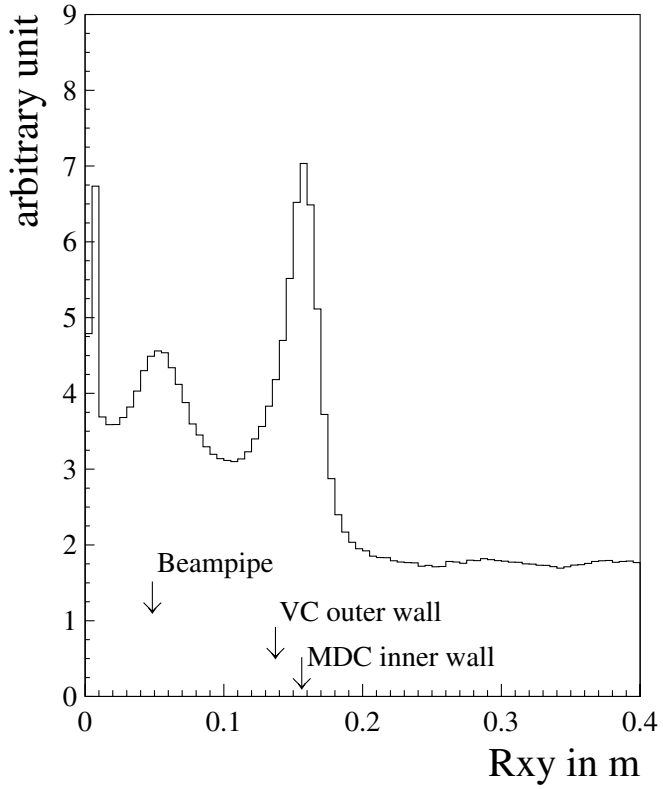


FIG. 1. The $R_{xy}$ distribution for candidate photon conversions to $e^+e^-$ pairs in the BESII detector from hadron events in the $58 \times 10^6$ $J/\psi$ event sample.

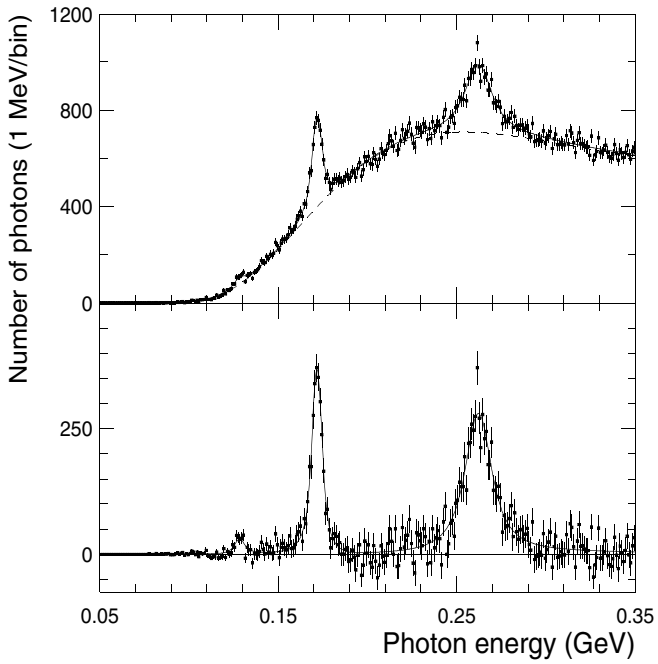


FIG. 2. Inclusive photon spectrum from photon conversions from $14 \times 10^6$ $\psi(2S)$ events. A fit (described in the text) is made to $\psi(2S) \to \gamma\chi_{cJ}$ decays ($J = 0, 1, 2$) plus background described by a threshold function. Points with error bars are data. The solid line is the fit; the dashed line is the fitted background. Background subtracted results are shown in the lower plot.

at the photon conversion point, and their momenta are corrected to that point.

Next good photons are selected. The photon conversion length must lie within the beam-pipe region, $2 < R_{xy} < 22$ cm, and the invariant mass of the candidate $e^+e^-$ pair is required to satisfy $M_{e^+e^-} < 20\ \mathrm{MeV}/c^2$. Hadron track pairs produced near the beam line are largely rejected by the $R_{xy}$ cut, and remaining hadron tracks from $K^0_S$ and $\Lambda$ decays are effectively suppressed by the $M_{e^+e^-}$ cut. Background from combinations of charged hadron tracks is further removed by requiring $\cos\theta_d > 0.9$, where $\theta_d$ is the angle between the photon momentum and photon track (a vector from the beam to the CP). In order to have high photon detection efficiency via photon conversions, especially for lower energy photons, neither electron identification nor any requirement on the $\chi_{cJ}$ decay is applied. To suppress background from beam-gas and beam-pipe interactions, the total energy in the event must satisfy $E_{\mathrm{tot}} > E_{\mathrm{beam}}/2$, and the momentum asymmetry must satisfy $p_{\mathrm{asym}} < 0.9$. Here $p_{\mathrm{asym}}$ is defined as a ratio of the vector sum to the scalar sum of the momenta of all charged and neutral tracks in the event. The observed photon energy spectrum from the $\psi(2S)$ data after the selection of good photons is shown in Fig. 2. The spectrum shows the $\chi_{cJ}$ states plus a large background. The sharp drop at low energy is caused mainly by low photon detection efficiency.

## IV. $dE/dx$ CORRECTION AND PHOTON ENERGY SCALE

Energy loss ($dE/dx$) by ionization for electrons traversing a small thickness of material with an energy above a few tens MeV can be described by the Bethe-Bloch equation [9]. The $dE/dx$ correction for charged particles, produced near the beam line and traversing the whole beam-pipe region, should take into account the full thickness of material in the region. However, $e^+e^-$ pairs from photon conversions are produced mostly in the region where the VC outer wall and the MDC inner wall are located. Thus, the effective thickness of material between the location, where a pair is produced, and first layer of the MDC wires must be estimated for each electron pair. The procedure to make $dE/dx$ corrections for electrons has two steps: (i) A preliminary $dE/dx$ correction using half the full thickness of the materials in the beam-pipe region is made for the fitted tracks and followed by determination of the intersection point and $R_{xy}$. (ii) The final $dE/dx$ corrections as a function of the $R_{xy}$, as well as the electron pair energies, are recalculated.

The energy scale of photons reconstructed from $e^+e^-$ pairs is studied using 503 $\pi^0$ mesons decaying to two

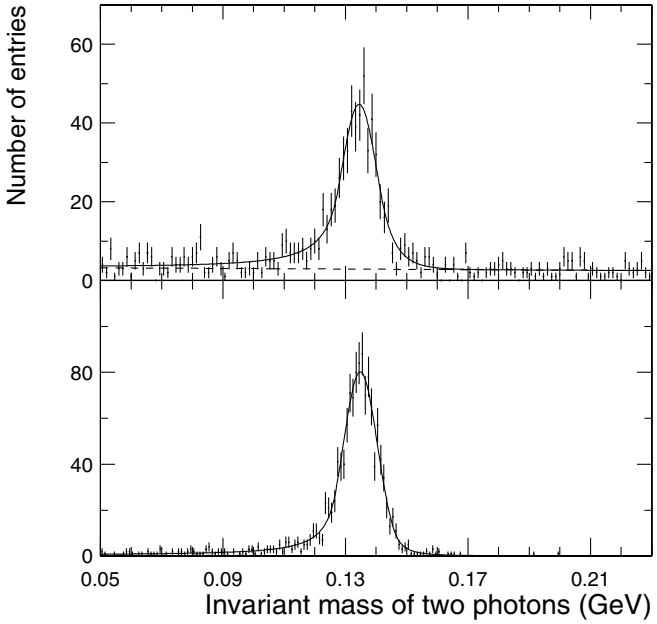


FIG. 3. Invariant mass distribution of a photon pair for $\pi^0 \to \gamma\gamma$ candidates with both photons converted to $e^+e^-$ pairs from $J/\psi$ data (top) and Monte Carlo (bottom) events. The solid lines are the fitted curves for signal plus background. The dashed lines are the fitted curves for background.

photons, with both photons converting to $e^+e^-$ pairs, selected from $58 \times 10^6$ $J/\psi$ events and $63 \times 10^6$ simulated $\pi^0$ events, generated with the same momentum and polar angular distributions as found from the $\pi^0$ data sample. To suppress hadron contamination, electron identification is required, and good photons are selected. A particle identification $\chi^2$ is calculated for each track for the electron, pion, kaon, and proton hypotheses using information from the MDC($dE/dx$), TOF, and BSC, and the associated probabilities are determined. A track is identified as an electron if the electron probability is greater than the probabilities for the pion, kaon, and proton hypotheses. Background is further suppressed with additional requirements on the photon energy, $E_\gamma \leq 1$ GeV, and the opening angle between the two photons, $0.75 < |\cos\theta_{\gamma\gamma}| < 0.97$. The invariant mass distribution of two photons for both MC and data, after the $dE/dx$ correction for electrons described above, is fitted with the improved Crystal Ball (ICB) function (defined in Sec. V) plus a first order polynomial background. The results are shown in Fig. 3. The resulting $\pi^0$ masses, $(134.47 \pm 0.42)$ MeV$/c^2$ in data and $(134.86 \pm 0.20)$ MeV$/c^2$ in MC data, are consistent with the PDG value of 134.98 MeV$/c^2$ [9]. The corresponding mass resolutions, $\sigma_{M_{\pi^0}} = (5.70 \pm 0.58)$ MeV$/c^2$ in data and $(5.55 \pm 0.21)$ MeV$/c^2$ in MC data, agree within errors. The $\chi^2$/D.F. (degree of freedom) for the fits are 126/103 in data and 117/140 in MC simulation.

## V. PROBABILITY DENSITY FUNCTION AND DETECTOR RESOLUTION

The energy of a photon from $\psi(2S) \to \gamma\chi_{cJ}$ decay is given by

$$E_\gamma = (M^2_{\psi(2S)} - M^2_{\chi_{cJ}})/2M_{\psi(2S)}, \quad (1)$$

where $M_{\psi(2S)}$ and $M_{\chi_{cJ}}$, described by Breit-Wigner functions, are the masses of the $\psi(2S)$ and $\chi_{cJ}$, respectively. Since both $M_{\psi(2S)}$ and $M_{\chi_{cJ}}$ appear as variables, this is a two-dimensional (2D) problem. Taking $x = M_{\psi(2S)}$, the probability density function (pdf) for the photon energy $E_\gamma$ can be written as [18]

$$f_{\rm pdf}(E_\gamma) = \int BW(x)BW(M_{\chi_{cJ}})\frac{x}{M_{\chi_{cJ}}}dx, \quad (2)$$

where $M_{\chi_{cJ}}$ depends on $E_\gamma$ by Eq. (1).

As a result of traversing material in the beam-pipe region, the electron energy is smeared due to energy loss by ionization, and a long tail on the low side of the energy

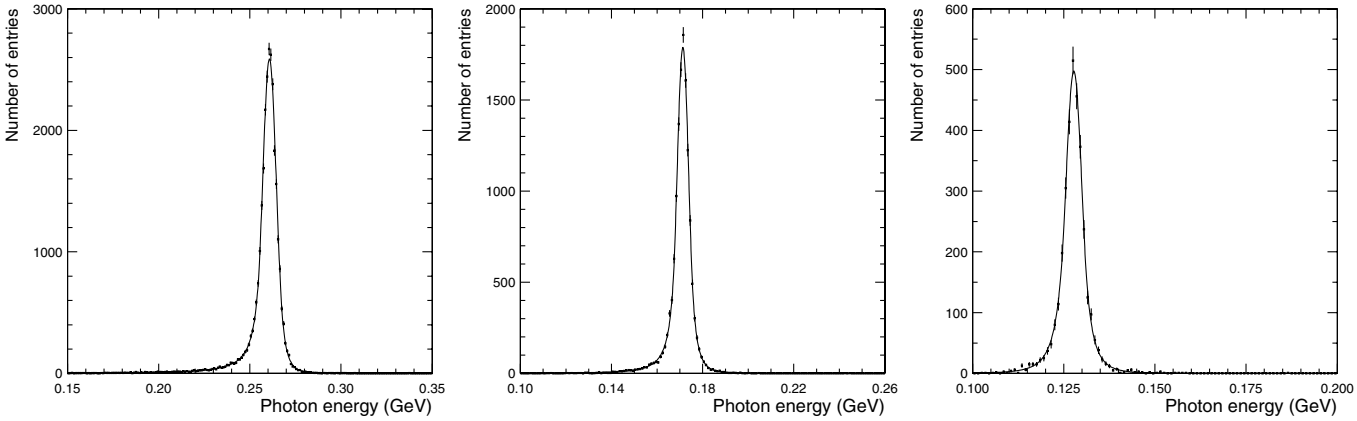


FIG. 4. Energy distributions of signal photons from $\psi(2S) \to \gamma\chi_{cJ}$ decays with zero widths for both $\psi(2S)$ and $\chi_{cJ}$ for $\chi_{c0}$ (left), $\chi_{c1}$ (middle), and $\chi_{c2}$ (right) final states fitted to the ICB function. The points are MC data. The solid lines are the fitted curves.

distribution is induced by bremsstrahlung radiation. Multiple scattering of electrons, especially with large-angle scatters, gives tails on both sides of the photon energy distribution of photon conversions. The photon energy resolution from photon conversions can be nicely modeled by our GEANT3 MC simulation and well fitted by the ICB function. The original Crystal Ball (CB) function has a Gaussian in its central and upper regions but a long tail in the lower region [19]. The improved CB function is defined as the same as the CB function but has an additional tail at its upper region. The photon energy distributions from large MC samples of $\psi(2S) \to \gamma\chi_{cJ}$ decays ($J = 0, 1, 2$), with zero widths for both the $\psi(2S)$ and $\chi_{cJ}$ states, are fitted to ICB functions and shown in Fig. 4. The $\chi^2$/D.F. from the fits are 103.8/93, 37.7/53, and 47.6/43 for the $\chi_{c0}$, $\chi_{c1}$, and $\chi_{c2}$ states, respectively. Five parameters in the ICB function, the photon energy resolution and four empirical parameters to describe the tails on the lower and upper sides, are determined from the fits and used as input parameters in the detector resolution function for each decay mode. Photon energy resolutions for the $\psi(2S) \to \gamma\chi_{cJ}$ decays ($J = 0, 1, 2$) are found to be $\sigma_{E_\gamma} = 3.78 \pm 0.04$, $2.58 \pm 0.05$, and $2.26 \pm 0.11$ MeV, respectively.

The energy dependencies of the photon detection efficiency and resolution are determined using MC simulation in the energy range between 100 and 400 (300, 220) MeV for $\psi(2S) \to \gamma\chi_{c0}(\gamma\chi_{c1}, \gamma\chi_{c2})$ decays. The efficiency includes the effects of detector geometry, MDC tracking, photon reconstruction, and the spin-dependent $\cos\theta$ distribution.

## VI. FITTING THE PHOTON SPECTRUM

Background contamination from $\chi_{c0} \to \gamma J/\psi$ decay is negligible due to its small branching fraction. To exclude photons from the $\chi_{c1,c2} \to \gamma J/\psi$ decays, the photon energy range in the fits is chosen to be $90\ \text{MeV} \le E_\gamma \le 350\ \text{MeV}$. Background from the decay $\psi(2S) \to \eta J/\psi$ with $\eta \to \gamma\gamma$ in the region from 180 to 400 MeV is subtracted from the data, using a shape estimated from MC simulation and normalized according to the measured total number of $\psi(2S)$ events and known branching fractions. The smooth background under the signal photon lines can be described by a threshold function from the *Mn_Fit* package [19].

$$bg_{\text{threshold}}(x) = B \cdot (x - x_0)^\alpha \cdot e^{c_1(x-x_0)+c_2(x-x_0)^2}, \quad (3)$$

where $B$, $x_0$, and $\alpha$ are normalization factor, threshold, and power; $c_1$ and $c_2$ are coefficients linear and quadratic in $x$. The threshold function has been used to fit background with a threshold at the lower or upper side of an observed distribution by experiments [20].

Considering the physical photon energy $x \equiv E_\gamma$ and its error $y \equiv \Delta E_\gamma$ due to detector resolution, the measured photon energy is $u = x + y$ and its pdf function can be written as:

$$\begin{aligned} h_{\text{pdf}}(u) &= \int c_{E_1}(u - y) \cdot c_{\text{eff}}(u - y) \cdot f_{\text{pdf}}(u - y) \\ &\quad \cdot g_{\text{res}}(y)dy \\ &= \int c_{E_1}(x) \cdot c_{\text{eff}}(x) \cdot f_{\text{pdf}}(x) \cdot g_{\text{res}x}(u - x)dx, \quad (4) \end{aligned}$$

where $c_{E_1}(x) = x^3/E^3_{\gamma,\chi_{cJ}}$, $c_{\text{eff}}(x) = \epsilon_{\chi_{cJ}}(x)/\epsilon(E_{\gamma,\chi_{cJ}})$, $f_{\text{pdf}}(x)$ is defined with Eq. (2), and $g_{\text{res}}(y)$ is the ICB resolution function. With the assumption that the $E1$ electric dipole transition for $\psi(2S) \to \gamma\chi_{cJ}$ decays ($J = 0, 1, 2$) dominates, an $E^3_\gamma$ energy dependence is included in the folded signal shape. The detection efficiency $\epsilon_{\chi_{cJ}}(x)$ and energy resolution as a function of photon energy are included in the fitting. Normalization factors $E_{\gamma,\chi_{cJ}}$ and $\epsilon(E_{\gamma,\chi_{cJ}})$ are the photon energies corresponding to fitted $\chi_{cJ}$ masses and efficiencies at these photon energies, respectively. The energies $E_{\gamma,\chi_{cJ}}$ are determined from the $\chi_{cJ}$ mass parameter values in fitting according to Eq. (1). The efficiencies $\epsilon(E_{\gamma,\chi_{cJ}})$ are calculated at the energies $E_{\gamma,\chi_{cJ}}$ and found to be 0.382%, 0.171%, and 0.0355% for the fitted $\chi_{c0}$, $\chi_{c1}$, and $\chi_{c2}$ masses, respectively. Note that the parameters, masses $M_{\chi_{cJ}}$, and widths $\Gamma_{\chi_{cJ}}$ ($J = 0, 1, 2$) are implicitly contained in the $f_{\text{pdf}}(x)$ function, and the detector resolution and tail parameters are in the $g_{\text{res}}(y)$ function. The likelihood function, $Lk(u; M_{\chi_{cJ}}, \Gamma_{\chi_{cJ}})$, is constructed with three $\chi_{cJ}$ signals plus threshold function background:

$$\begin{aligned} Lk(u; M_{\chi_{cJ}}, \Gamma_{\chi_{cJ}}) &= bg_{\text{threshold}}(u) + \sum_{J=0}^{2} A_J \\ &\quad \cdot h_{\text{pdf},\chi_{cJ}}(u; M_{\chi_{cJ}}, \Gamma_{\chi_{cJ}}). \quad (5) \end{aligned}$$

Here $A_J$ is the observed area in each $\chi_{cJ}$ signal.

An input-output test is performed to verify the accuracy of the fitting algorithm for the 2D problem using MC events. The energy dependencies of the photon detection efficiency and resolution are included in the fitting procedure. A sample of MC events for the $\psi(2S) \to \gamma\chi_{cJ}$ decays with nonzero width for both the $\psi(2S)$ and $\chi_{cJ}$ are produced. The photon energy distribution is fitted with the 2D pdf function convoluted with the ICB resolution. The resulting masses and widths of the $\chi_{cJ}$ states in this test are consistent with the MC input parameters.

A combined fit of the three photon spectra corresponding to the $\psi(2S) \to \gamma\chi_{c0}, \gamma\chi_{c1}, \gamma\chi_{c2}$ decays is performed to three 2D pdf functions [see Eq. (2)], each convoluted with its ICB resolution function, plus threshold function background. The $\chi_{c2}$ width is fixed in the fit due to the limited statistics. The $\chi^2$ and D.F. from the fit are 521.0 and (520-13), where the total number of free parameters is 13. The effect of the beam energy spread [21] in the measurement is also included but is found to be negligible due to the narrow width of the $\psi(2S)$ state. A study shows that the bin size (0.5 or 0.2 MeV) in the binned fits slightly affects

TABLE I. Results from the combined fit of the three photon spectra corresponding to the $\psi(2S) \to \gamma\chi_{c0}, \gamma\chi_{c1}, \gamma\chi_{c2}$ plus threshold function background. The definition of fit parameters is described in the text [see Eqs. (3) and (5)].

| Parameter | Fitted result |
|---|---|
| $A_{\chi_{c0}}$ | $(655 \pm 48) \times 10$ |
| $M_{\chi_{c0}}$ | $3414.21 \pm 0.39$ MeV/$c^2$ |
| $\Gamma_{\chi_{c0}}$ | $12.6^{+1.5}_{-1.6}$ MeV/$c^2$ |
| $A_{\chi_{c1}}$ | $(300 \pm 15) \times 10$ |
| $M_{\chi_{c1}}$ | $3510.30 \pm 0.14$ MeV/$c^2$ |
| $\Gamma_{\chi_{c1}}$ | $1.39^{+0.40}_{-0.38}$ MeV/$c^2$ |
| $A_{\chi_{c2}}$ | $227 \pm 40$ |
| $M_{\chi_{c2}}$ | $3555.70 \pm 0.59$ MeV/$c^2$ |
| $\Gamma_{\chi_{c1}}$ | 2.11 MeV/$c^2$ (fixed) |
| $B$ | $(1.43 \pm 0.32) \times 10^{14}$ |
| $x_0$ | $(7.23 \pm 0.11) \times 10^{-2}$ |
| $\alpha$ | $6.38 \pm 0.08$ |
| $c_1$ | $-55.5 \pm 1.0$ |
| $c_2$ | $56.1 \pm 2.3$ |

the fitted masses and widths of the $\chi_{cJ}$ states. The difference in the results due to different bin sizes is added to the systematic error. The results of the binned fit (0.5 MeV/bin) are shown in Fig. 2, and resulting parameter values are listed in Table I. The correlation coefficients between the $\chi_{cJ}$ masses in the resulting error matrix are found to be small: $-0.002$ between $\chi_{c0}$ and $\chi_{c1}$ masses, 0.001 between $\chi_{c0}$ and $\chi_{c2}$ masses, and $-0.008$ between $\chi_{c1}$ and $\chi_{c2}$ masses.

## VII. SYSTEMATIC ERRORS

Samples of QED radiative two photon events with one photon converting to an $e^+e^-$ pair are selected for both data and MC simulation. The two photons are required to be emitted back to back. The fitted photon energy in data is different from the expected MC value by $-1.2\sigma$ ($\sigma = 0.86$ MeV), which has a relative error at the same level as a correction factor $s = 0.9975 \pm 0.0007$ for the magnetic field [22]. Thus, a relative precision of 0.0007 is added as the systematic error in the photon energy determination.

The $\pi^0$ mass resolutions determined from the data and MC are in good agreement; their difference is $0.15 \pm 0.62$ MeV/$c^2$. We assume that the photon energy resolution and uncertainty in the direction of the photon momentum each contribute half in the $\pi^0$ mass resolution. Hence, the difference $\Delta\sigma_{M_{\pi^0}}$ of the $\pi^0$ mass resolutions between MC and data from the uncertainty of the photon energy resolution lies within $(-0.29, +0.59)$ MeV/$c^2$ with a probability of 68.3%. We assume $\Delta\sigma_{E_\gamma}(\chi_{cJ})/\sigma_{E_\gamma}(\chi_{cJ}, \mathrm{MC}) = \Delta\sigma_{M_{\pi^0}}/\sigma_{M^0_\pi}(\mathrm{MC})$, where $\sigma_{E_\gamma}(\chi_{cJ}, \mathrm{MC})$ and $\Delta\sigma_{E_\gamma}(\chi_{cJ})$ are the MC photon energy resolution and the difference between MC and data for $\chi_{cJ}$ final states, respectively, and $\sigma_{M^0_\pi}(\mathrm{MC})$ and $\Delta\sigma_{M_{\pi^0}}$ are $\pi^0$ mass resolution in MC and the difference between MC and data, respectively. Thus, $1\sigma$ confidence intervals of $\Delta\sigma_{E_\gamma}(\chi_{cJ})$ for the $\psi(2S) \to \gamma\chi_{c0}, \gamma\chi_{c1}$ decays are estimated to be $(-0.20, +0.40)$ and $(-0.14, +0.27)$ MeV, which are used to estimate systematic errors in the determination of the $\chi_{c0}$ and $\chi_{c1}$ widths.

TABLE II. Summary of systematic errors in the determination of the $\chi_{cJ}$ masses and widths (in MeV/$c^2$).

| Source | $M_{\chi_{c0}}$ | $\Gamma_{\chi_{c0}}$ | $M_{\chi_{c1}}$ | $\Gamma_{\chi_{c1}}$ | $M_{\chi_{c2}}$ |
|---|---|---|---|---|---|
| Background shape | 0.03 | 0.8 | 0.02 | 0.07 | 0.04 |
| Correction in magnetic field | 0.19 | | 0.13 | | 0.09 |
| MC simulation in $\sigma_{E_\gamma}$ | | $^{+0.29}_{-0.76}$ | | $^{+0.25}_{-0.77}$ | |
| Different bin size | 0.02 | 0.02 | 0.01 | 0.01 | 0.02 |
| Photon energy correction | 0.18 | | 0.09 | | 0.37 |
| Efficiency uncertainty | 0.04 | 0.03 | 0.01 | 0.00 | 0.04 |
| Error of $M_{\psi(2S)}$ | 0.034 | | 0.034 | | 0.034 |
| Total | 0.27 | $^{+0.85}_{-1.10}$ | 0.16 | $^{+0.26}_{-0.77}$ | 0.39 |

The effect of the background shape uncertainty is studied using $\psi(2S)$ data and $\psi(2S) \to$ anything MC [23]. The relative differences in background shape parameters between floated and fixed widths of the $\chi_{c0,c1}$ states are determined in fits for MC data and fed back to correct background parameters in the fits for data. The difference between results for $\psi(2S)$ data with the background shape floated and fixed is taken as a systematic error. In addition, our MC study with nonzero width of both $\psi(2S)$ and $\chi_{cJ}$ shows that differences in the fitted masses from input values for the $\chi_{c0}$ and $\chi_{c1}$ are $0.12 \pm 0.06$ and $0.06 \pm 0.03$ MeV/$c^2$, respectively, while that for the $\chi_{c2}$ is as large as $0.31 \pm 0.06$ MeV/$c^2$. The differences are attributed to uncertainties in the energy loss correction for low momentum electrons. The systematic errors, including the contributions from the uncertainties of the photon detection efficiency, are summarized in Table II.

## VIII. RESULTS AND DISCUSSION

With good energy resolution for low energy photons obtained using photon conversions, the precise measurement of the masses and widths of $\chi_{cJ}(J = 0, 1, 2)$ states from inclusive $\psi(2S)$ radiative decays can be obtained. The masses and widths are determined to be $M_{\chi_{c0}} = 3414.21 \pm 0.39 \pm 0.27$, $M_{\chi_{c1}} = 3510.30 \pm 0.14 \pm 0.16$, $M_{\chi_{c2}} = 3555.70 \pm 0.59 \pm 0.39$ MeV/$c^2$, $\Gamma_{\chi_{c0}} = 12.6^{+1.5+0.9}_{-1.6-1.1}$, and $\Gamma_{\chi_{c1}} = 1.39^{+0.40+0.26}_{-0.38-0.77}$ MeV/$c^2$. The mass splittings in the $\chi_{cJ}(1P)$ triplet and their ratio are found to be $\Delta M_{21} = M_{\chi_{c2}} - M_{\chi_{c1}} = 45.40 \pm 0.61 \pm 0.42$ MeV/$c^2$, $\Delta M_{10} = M_{\chi_{c1}} - M_{\chi_{c0}} = 96.09 \pm 0.41 \pm 0.31$ MeV/$c^2$, and $\rho(\chi_c) = \Delta M_{21}/\Delta M_{10} = 0.472 \pm 0.006 \pm 0.004$. The spin-averaged $^3P_J$ mass (weighted with factors $2J + 1$) for the $\chi_{cJ}$ states is measured precisely in one experiment and determined to be $M(^3P_{\mathrm{cog}}) = 3524.85 \pm 0.32 \pm 0.30$ MeV/$c^2$.

TABLE III. Mass splittings in the $\chi_{cJ}(1P)$ triplet and their ratio $\rho$, and spin-averaged $^3P_J$ mass $M(^3P_{\rm cog})$ for the $\chi_{cJ}$ states measured by BES. CLEO [11] and E835 [24] are listed for comparison.

| Parameter | BES | CLEO | E835 |
|---|---|---|---|
| $\Delta M_{21}$ in MeV/$c^2$ | $45.40 \pm 0.61 \pm 0.42$ | | $45.45 \pm 0.15$ |
| $\Delta M_{10}$ in MeV/$c^2$ | $96.09 \pm 0.41 \pm 0.31$ | | $95.2 \pm 0.6$ |
| $\rho$ | $0.472 \pm 0.006 \pm 0.004$ | $0.490 \pm 0.002 \pm 0.003$ | $0.477 \pm 0.002$ |
| $M(^3P_{\rm cog})$ in MeV/$c^2$ | $3524.85 \pm 0.32 \pm 0.30$ | | $3525.39 \pm 0.10$ |

The first errors in the results are statistical, and the second are systematic. Correlations are taken into account in estimations of both statistical and systematic errors for the $\Delta M_{21}$, $\Delta M_{10}$, $\rho(\chi_c)$, and $M(^3P_{\rm cog})$. Correlation coefficients between mass parameters for the statistical error are obtained from the error matrix of the combined fit. The systematic error for the $M(^3P_{\rm cog})$ with correlations is 0.30 MeV/$c^2$, assuming all correlation coefficients between mass parameters are equal to 100% as a conservative estimation and that added in quadrature without correlations is 0.21 MeV/$c^2$.

The $\chi_{cJ}$ masses ($J = 0, 1, 2$) determined here are consistent with the recent measurements by CLEO [11] but have smaller systematic errors. The precisions for the $\chi_{c0}$ and $\chi_{c1}$ masses are compatible with those of previous measurements by E835 [10] and E760 [9], while that for the $\chi_{c2}$ mass is not as good as theirs due to low statistics. Note that our $\chi_{c0}$ mass is lower than that measured by E835 via $\chi_{c0} \to \gamma J/\psi$ decay by 1.2 MeV (corresponding to $1.8\sigma$) but agrees with their later measurement via $\chi_{c0} \to \pi^0\pi^0$ decay. The widths of the $\chi_{cJ}$ states ($J = 0, 1$) determined here are also consistent with their values; larger errors in our widths are caused by limited statistics for both signal photons and inclusive $\pi^0$ mesons in the data samples.

Subsequent to the submission of this paper, similar results from E835 became available [24]. Our result on the masses and widths of the $\chi_{c1}$ and $\chi_{c2}$ states, as well as the mass splittings in the $\chi_{cJ}(1P)$ triplet and the spin-averaged $^3P_J$ mass, agree well with their new precise results (see Table III).

## ACKNOWLEDGMENTS

The BES Collaboration thanks the staff of BEPC for their hard efforts, the members of IHEP computing center for their helpful assistance, and also T. P. Li for helpful discussion on 2D pdf function. This work is supported in part by the National Natural Science Foundation of China under Contracts No. 19991480, No. 10225524, and No. 10225525, the Chinese Academy of Sciences under Contract No. KJ 95T-03, the 100 Talents Program of CAS under Contracts No. U-11, No. U-24, and No. U-25, and the Knowledge Innovation Project of CAS under Contracts No. U-602 and No. U-34 (IHEP); by the National Natural Science Foundation of China under Contract No. 10175060 (USTC) and No. 10225522 (Tsinghua University); and by the U.S. Department of Energy under Contract No. DE-FG02-04ER41291 (University of Hawaii).

[1] E. Eichten *et al.*, Phys. Rev. D **21**, 203 (1980); **17**, 3090 (1978); V. A. Novikov, *et al.*, Phys. Rep. **41**, 1 (1978); C. Quigg and J. L. Rosner, Phys. Rep. **56**, 167 (1979); G. Bali, K. Schilling, and A. Wachter, Phys. Rev. D **56**, 2566 (1997).

[2] S. K. Choi *et al.* (Belle Collaboration), Phys. Rev. Lett. **91**, 262001 (2003); B. Aubert *et al.* (*BABAR* Collaboration), Phys. Rev. D **71**, 071103 (2005).

[3] S. K. Choi *et al.* (Belle Collaboration), Phys. Rev. Lett. **89**, 102001 (2002); A. Tomaradze, hep-ex/0410090; C. Patrignani, hep-ex/0410085.

[4] N. Brambilla *et al.*, hep-ph/0412158.

[5] D. Ebert, R. N. Faustov, and V. O. Galkin, Phys. Rev. D **67**, 014027 (2003); **62**, 034014 (2000).

[6] S. F. Radford and W. W. Repko, hep-ph/0409290.

[7] A. S. Artamonov *et al.* (OLYA and MD-1 Collaborations), Phys. Lett. B **474**, 427 (2000).

[8] V. M. Aulchenko *et al.* (KEDR Collaboration), Phys. Lett. B **573**, 63 (2003); J. Z. Bai *et al.* (BES Collaboration), Phys. Lett. B **550**, 24 (2002).

[9] S. Eidelman *et al.* (Particle Data Group), Phys. Lett. B **592**, 1 (2004).

[10] S. Bagnosco *et al.* (E835 Collaboration), Phys. Lett. B **533**, 237 (2002); M. Andreotti *et al.*, Phys. Rev. Lett. **91**, 091801 (2003).

[11] S. B. Athar *et al.* (CLEO Collaboration), Phys. Rev. D **70**, 112002 (2004). From their measured photon energies, one may estimate the $\chi_{cJ}$ masses using Eq. (1) in the text.

[12] S. Godfrey and J. L. Rosner, Phys. Rev. D **66**, 014012 (2002); S. Godfrey, hep-ph/0501083.

[13] J. Z. Bai *et al.* (BES Collaboration), Nucl. Instrum. Methods Phys. Res., Sect. A **458**, 627 (2001); **344**, 319 (1994).
[14] G. S. Huang *et al.* (BES Collaboration), High Energy Phys. Nucl. Phys. **25**, 889 (2001), in Chinese; Fu Chengdong, ''*Measurement of the Trigger Efficiency for psi(2S) Data*,'' BES internal report, 2003.
[15] H. M. Liu *et al.*, ''The BESII Detector Simulation'' (unpublished).
[16] G. Karl, S. Meshkov, and J. L. Rosner, Phys. Rev. D **13**, 1203 (1976).
[17] T. Hong *et al.*, High Energy Phys. Nucl. Phys. **25**, 617 (2001).
[18] M. Fisz, *Probability and Mathematic Statistics* (VEB Deutscher Verlag der Wissenschaften, Berlin, 1958).
[19] I. C. Brock, A Fitting and Plotting Package Using MINUIT, version 4.07, 2000.
[20] For instance, see B. Aubert *et al.* (*BABAR* Collaboration), Phys. Rev. D **65**, 091104 (2002).
[21] The spread in the center-of-mass energy at $\psi(2S)$ energy is 1.3 MeV. See also J. Z. Bai *et al.* (BES Collaboration), Phys. Lett. B **550**, 24 (2002).
[22] A correction factor $s = 0.9975 \pm 0.0007$ for magnetic field at the BESII is determined with mass measurement of the $J/\psi$ reconstructed from $\psi(2S) \rightarrow \pi^+\pi^- J/\psi$ and $J/\psi \rightarrow \mu^+\mu^-$ decays.
[23] J. C. Chen *et al.*, Phys. Rev. D **62**, 034003 (2000).
[24] A new measurement by E835 appeared soon after this paper. See M. Andreotti *et al.*, hep-ex/0503022.